Chinese Chemical Letters 33 (2022) 2663–2668

Contents lists available at ScienceDirect

Chinese Chemical Letters

journal homepage: www.elsevier.com/locate/cclet

Pre-potassiated hydrated vanadium oxide as cathode for *quasi*-solid-state zinc-ion battery

Qifei Li[a], Xiangxiang Ye[a], Hong Yu[b,*], Chengfeng Du[b], Wenping Sun[c,d], Weiling Liu[e], Hongge Pan[c,d], Xianhong Rui[a,*]

[a] School of Materials and Energy, Guangdong University of Technology, Guangzhou 510006, China
[b] Center of Advanced Lubrication and Seal Materials, Northwestern Polytechnical University, Xi'an 710072, China
[c] Institute of Science and Technology for New Energy, Xi'an Technological University, Xi'an 710021, China
[d] School of Materials Science and Engineering, State Key Laboratory of Silicon Materials, Zhejiang University, Hangzhou 310027, China
[e] School of Materials Science and Engineering, Nanyang Technological University, Singapore 639798, Singapore

ARTICLE INFO

Article history:
Received 22 July 2021
Revised 11 September 2021
Accepted 25 September 2021
Available online 30 September 2021

Keywords:
Quasi-solid-state
Zinc-ion batteries
Hydrated vanadium oxide
Pre-potassiated
Electrochemical kinetics

ABSTRACT

Zinc-ion batteries (ZIBs), in particular *quasi*-solid-state ZIBs, occupy a crucial position in the field of energy storage devices owing to the superiorities of abundant zinc reserve, low cost, high safety and high theoretical capacity of zinc anode. However, as divalent Zn^{2+} ions experience strong electrostatic interactions when intercalating into the cathode materials, which poses challenges to the structural stability and higher demand in Zn^{2+} ions diffusion kinetics of the cathode materials. Here, a microwave-assisted hydrothermal method is adopted to prepare pre-potassiated hydrated vanadium pentoxide ($K_{0.52}V_2O_5{\cdot}0.29H_2O$, abbreviated as KHVO) cathode material, in which the potassium ions pre-inserted into the interlayers can act as "pillars" to stabilize the lamellar structure, and crystal water can act as "lubricant" to improve the diffusion efficiency of Zn^{2+} ions. Consequently, the KHVO displays high electrochemical properties with high capacity (~300 mAh/g), superior rate capability (69 mAh/g at 5 A/g) and ultralong cycling performance (>1500 cycles at 2 A/g) in *quasi*-solid-state ZIBs. These superior Zn storage properties result from the large diffusion coefficient and highly stable and reversible Zn^{2+} (de)intercalation reaction of KHVO.

Zinc-ion batteries (ZIBs) are attracting numerous attentions as a promising candidate for future energy storage devices ascribing to the abundant zinc resource, high safety and low cost [1–6]. In particular, *quasi*-solid-state ZIBs with better flexibility, high compatibility with flexible electronics and higher inhibition of Zn dendrites have become the hotspot of research [7–10]. Nevertheless, the strong electrostatic forces experienced by the moving divalent Zn^{2+} ions in the cathode materials raise difficulties in the repetitive Zn^{2+} insertion/extraction reaction and cause structural distortion/failure, and thus resulting in unsatisfying electrochemical performance [11]. Therefore, seeking and optimizing cathode materials with rigid structure stability and excellent Zn^{2+} (de)intercalation kinetics has become a priority as well as a challenge for the development of ZIBs.

Up to now, the researches of cathode materials for ZIBs are mainly focused on Mn-based materials [12–15], Prussian blue analogs [16–19], and V-based materials [20–24]. Among them, the Mn-based materials always suffer from rapid capacity attenuation during the repeated charging and discharging processes, deriving from the irreversible phase transition and Mn dissolution [25–27]. As for Prussian blue analogs, the capacity (< 100 mAh/g) is too low to meet the requirements for practical application. Considering these facts, great devotion has been paid to the study of V-based materials as cathodes for ZIBs. V-based materials can exhibit a large Zn storage capacity of ~400 mAh/g due to the variable chemical states of vanadium ions between +5 and +3. And they usually possess layered or tunnel structures with large inner spaces that allow rapid diffusion of Zn^{2+} ions. Additionally, the vanadium element is very rich in natural resources, which further reduces the cost.

Among all the V-based materials, the layered hydrated vanadium pentoxide ($V_2O_5{\cdot}mH_2O$, named as HVO) is of great potential as cathode for ZIBs, in which the expanded interlayer distances (~12 Å) caused by structural water molecules efficiently promote the diffusion and storage of Zn^{2+} ions [28–30]. However, the HVO material is still beset by poor structural stability dur-

* Corresponding authors.
E-mail addresses: yh@nwpu.edu.cn (H. Yu), xhrui@gdut.edu.cn (X. Rui).

https://doi.org/10.1016/j.cclet.2021.09.091
1001-8417/

ing the process of repeated Zn^{2+} ions insertion/extraction [31,32]. For instance, Sun *et al.* developed a binder-free $V_2O_5{\cdot}nH_2O$/reduced graphene oxide film as the solid-state ZIBs cathode [33], which showed a rapid capacity decay when cycling at 0.1 A/g (capacity retention of 28% after 100 cycles). Xu *et al.* fabricated a 3D flower-like $V_2O_5{\cdot}nH_2O$/MXene composite as aqueous ZIBs cathodes [34]. Although electrical conductivity of the composite was enhanced, the electrochemical property was still hampered by the sluggish Zn^{2+} ion diffusion and ineffective utilization (capacity retention of 69% after 50 cycles at 0.1 A/g). To address this inherently low structural stability and enhance the Zn^{2+} ion diffusion kinetics of HVO, a foreign cation pre-intercalation method is proposed. The foreign cations can act as "pillar" that not only stabilize the layered structure of the material, but also enhance its electrical conductivity. HVO with various foreign cations pre-intercalated in the interlayer spacing have been investigated, such as Na^+ [35], Ca^{2+} [36], Zn^{2+} [37], Mg^{2+} [29], Mn^{2+} [30], Ni^{2+} [38], NH_4^+ [39], La^{3+} [40]. For example, $Mg_{0.34}V_2O_5{\cdot}nH_2O$ nanobelts were designed and prepared by Ming *et al.* [29], which showed an enhanced cycling performance (negligible capacity decay at 0.1 A/g during 200 cycles, and ~97% capacity retention at 5 A/g after 2000 cycles). Liu *et al.* proposed Mn(II)-cation-expanded hydrated vanadium pentoxide [30], delivering a ultrastable cycling performance (96% capacity retention at 4 A/g after 2000 cycles). All these researches proved the effectiveness in enhancing the electrochemical performance of HVO by introduction of foreign cations and points out the direction for further in-depth investigations.

Inspired by these intriguing properties, we developed a simple microwave-assisted hydrothermal route to synthesize pre-potassiated hydrated vanadium pentoxide ($K_xV_2O_5{\cdot}nH_2O$, named as KHVO) nanobelts, which are intertwined with each other to form a wrinkled three-dimensional (3D) structure. The KHVO material shares a similar layered structure with hydrated vanadium pentoxide, and the K^+ ions in the interlayer serve as "pillars" to stabilize the lamellar structure. It possesses a large interlayer spacing (~10.4 Å) along *c* axis, which makes the diffusion of Zn^{2+} ions effortless. Supported by all these advantages, the KHVO cathode achieves an enhanced zinc storage property in *quasi*-solid-state ZIBs, specifically a relatively high reversible capacity of ~300 mAh/g at 100 mA/g, acceptable rate capability of 65 mAh/g at 5 A/g and ultrastable long-term cycling performance (>1500 cycles at 2 A/g).

Through a simple microwave-assisted hydrothermal route, the KHVO material was prepared. Firstly, 3 mmol of vanadium pentoxide (V_2O_5) and 3 mL of 30% hydrogen peroxide (H_2O_2) solution were dissolved in deionized water (30 mL) and magnetic stirred for 20 min. After a homogeneous reddish-brown solution was formed, 6 mmol of potassium chloride (KCl) was weighed and poured into the above solution and kept stirring for a while. Afterward, the obtained solution was sealed in reactors and reacted for 2 h at 180 °C. After this hydrothermal process, the obtained product was washed with deionized water and absolute ethanol repeatedly and dried for 12 h at 60 °C vacuum oven.

The control HVO material was prepared by a simple hydrothermal according to the previous literature [31]. 0.32 g of ammonium metavanadate (NH_4VO_3) was blended with 80 mL of mixed solvent of deionized water and ethanol (9:1, v/v), and the pH value of mixture was reduced to 2 using hydrochloric acid (HCl). After that, the resulting solution was loaded into a 100 mL reactor and kept at 160 °C for 12 h to form $V_2O_5{\cdot}mH_2O$.

The phase of the sample was analyzed by X-ray powder diffraction (XRD) measurement (Bruker, AXS D8 advance, Cu Kα radiation). The field-emission scanning electron microscopy (FESEM, JEOL, Model JSM-7600F) and the transmission electron microscopy (TEM, JEOL, Model JEM-2100) technologies were applied to investigated the morphology and nanostructure of the sample. The valence states of various constituent elements were investigated by the X-ray photoelectron spectroscopy (XPS, Thermo Fisher, Model ESCALAB 250 Xi). The ratio of pre-intercalated potassium element to vanadium element in the sample was confirmed by inductively coupled plasma (ICP, Thermo Fisher, Model ICAP RQ). For the target of measuring the content of crystal water, thermal gravimetric analyzer (TGA, Mettler Toledo, Model DSC3+) was applied.

The Zn^{2+} ion storage properties of KHVO materials were evaluated in the *quasi*-solid-state zinc ion batteries. The cathode slurry was made of active material, carbon nanotube (CNT) and poly-(vinyldifluoride) (PVDF) in the mass ratio of 7:2:1 in *N*-methylpyrrolidone (NMP) solvent. Then, the electrode was prepared by coating the above slurry on titanium foil (diameter: 12 mm) and drying it in vacuum oven under 70 °C for more than 12 h. The mass loading of active material is controlled to ~1 mg/cm^2. The *quasi*-solid-state polymer membrane was prepared as follows: (1) adding 750 mg of PVDF polymer and 1 mmol of $Zn(ClO_4)_2$ salt in 10 mL of *N*-dimethylformamide (DMF) solvent under magnetic stirring to form homogeneous solution; (2) pouring the obtained solution into a mold with a diameter of 90 mm and drying it at vacuum oven for 8 h under 80 °C; (3) cutting the dried membrane into 16 mm diameter discs and soaking them into 0.5 mol/L $Zn(ClO_4)_2$ in propylene carbonate (PC) solution for 24 h; (4) removing the excess electrolyte completely before the usage. The *quasi*-solid-state ZIBs were assembled with obtained KHVO cathode, zinc foil and above polymer membrane in the air. The galvanostatic charging-discharging tests were carried out using NEWARE battery system during the voltage range of 0.4–1.4 V *vs.* Zn^{2+}/Zn. The cyclic voltammetry (CV) and electrochemical impedance spectroscopy (EIS) tests within the frequency ranging from 100 kHz to 0.01 Hz were evaluated by CHI660E electrochemical station. For comparison, the liquid-state ZIBs was also evaluated using glass fiber and 0.5 mol/L $Zn(ClO_4)_2$ in PC solvent as membrane and electrolyte, respectively.

The HVO and KHVO were fabricated through a facile traditional and microwave-assisted hydrothermal route, respectively, whose structures were confirmed by X-ray powder diffraction (XRD) measurements. The HVO sample (Fig. S1 in Supporting information) depicts a set of diffraction peaks corresponding to a set of planes along the *z*-axis of the layered $V_2O_5{\cdot}mH_2O$, revealing a preferred orientation along the (001) plane [29–31,33]. While for the XRD pattern of KHVO nanobelts in Fig. 1a, a few additional peaks are detected other than the major peaks along the (00*l*) direction ascribing to the intercalation of K^+ ions in the interlayers forming $K_xV_2O_5{\cdot}mH_2O$ phase as reported in previous studies [28,38,41,42]. As illustrated in the inset of Fig. 1a, the KHVO has a layered structure, where the bilayered chains of VO_5 pyramids are connected by the corner-sharing O atoms and accommodate the K^+ ions and H_2O molecular between the interlayers. And according to Bragg's law, the diffraction peak at 8.5° for the (001) plane is calculated with an interlayer distance to be as large as 10.4 nm, providing sufficient spaces for rapid diffusion of Zn^{2+} ions in the KHVO sample.

To explore the elemental compositions and chemical states of the KHVO sample, X-ray photoelectron spectroscopy (XPS) measurements were carried out. The survey confirms the existence of V, O and K elements (Fig. 1b). Fig. 1c shows the high-resolution spectrum of O 1s and V 2p region for the KHVO sample. Two states of O 1s at 531.6 eV for H–O and 530.7 eV for V–O can be differentiated, deriving from crystal water and VO layer, respectively [42]. In the V $2p_{3/2}$ region, the main characteristic peak located at 517.8 eV is identified to be V^{5+}. A relatively weak characteristic peak located at 516.7 eV is also detected, which indicates the presence of V^{4+} resulted from the K^+ ions pre-intercalation [43]. And K 2p re-

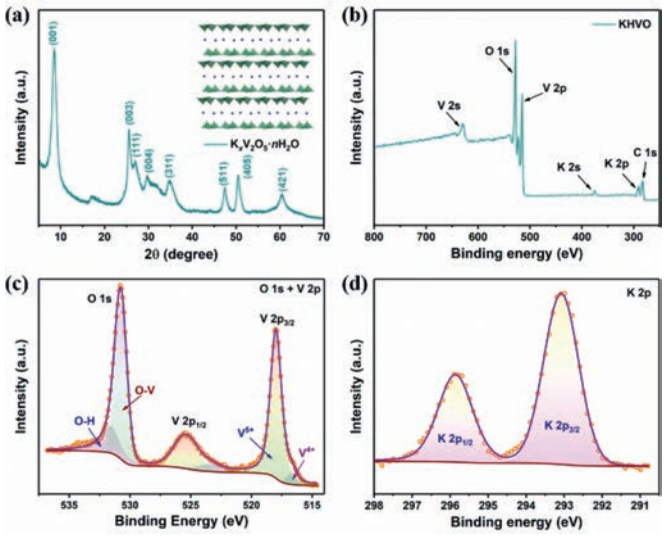

Fig. 1. (a) XRD pattern of KHVO (inset: schematic diagram of crystal structure, green and red balls stand for V and O, respectively, and blue balls stand for K and H_2O molecule). (b) XPS survey of KHVO and respective high-resolution spectra of (c) O 1s and V 2p and (d) K 2p.

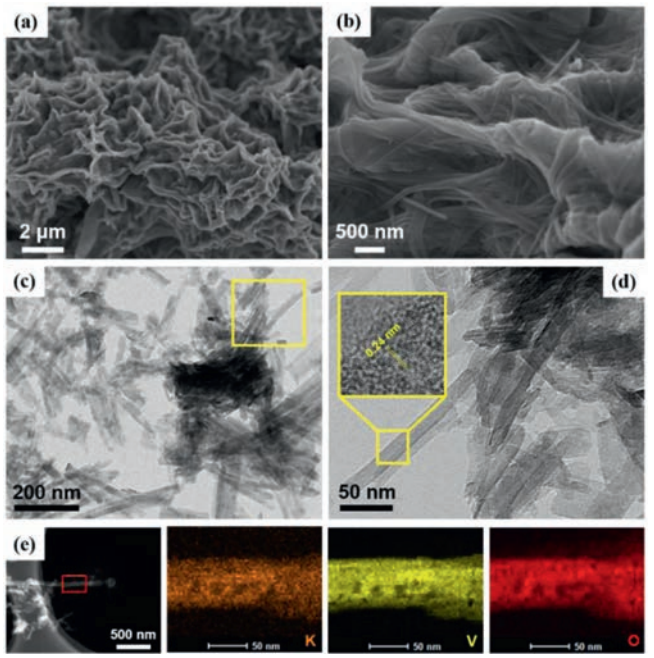

Fig. 2. (a, b) SEM images, (c, d) TEM images (inset: high-magnification TEM) and (e) dark-field STEM image and corresponding K, V and O elemental EDS mapping of KHVO.

gion of KHVO sample is also provided in Fig. 1d, which shows two peaks located at 295.9 and 293.1 eV, belonging to the K $2p_{1/2}$ and K $2p_{3/2}$, respectively [44,45].

Furthermore, to measure the content of K element and crystal water in the KHVO sample, inductively coupled plasma (ICP) and thermal gravimetric analysis (TGA) were conducted. According to the ICP test, the atomic ratio of K to V is determined to be 0.26:1, corresponding to a formula of $K_{0.52}V_2O_5{\cdot}nH_2O$. The TG analysis results are given in Fig. S2 (Supporting information). The rapid weight loss of both samples under 100 °C comes from the volatilization of physically absorbed water. As the temperature increases further, for KHVO sample, 2.3% of weight loss occurs, which is caused by the loss of structural water, implying that n is ~0.29 and thus $K_{0.52}V_2O_5{\cdot}0.29H_2O$. In the same way, the crystal water content in HVO sample is calculated to be 8.8%, fixing the formula as $V_2O_5{\cdot}0.94H_2O$.

Scanning electron microscope (SEM) and transmission electron microscope (TEM) tests were conducted to observe the morphology and microstructure of both samples. The low-magnification SEM image (Fig. S3a in Supporting information) of the HVO sample displays the uniformly distributed nanobelt morphology with a length of tens of micrometers. An enlarged view in Fig. S3b (Supporting information) reveals the width of the HVO nanobelts to be 60–100 nm. While for the KHVO sample, a wrinkled three-dimensional (3D) structure morphology (Figs. 2a and b) is observed, in which the micron-sized nanobelts are cross-linked and intertwined. Moreover, the TEM images (Figs. 2c and d, Fig. S4 in Supporting information) reveal the width of the nanobelts is around 20–50 nm. Zooming in the nanobelt in the marked area in Fig. 2d, the high-resolution TEM (HRTEM) picture in the inset shows a lattice fringe of 0.24 nm, corresponding to the diffraction peak at ~34° (311) in XRD pattern. Additionally, the dark-field scanning TEM (STEM) image and its respective energy-dispersive X-ray spectroscopy (EDS) element mapping images in Fig. 2e exhibit the uniform distribution of K, V and O elements in KHVO nanobelt.

Zinc storage performance of the KHVO as cathode materials was evaluated in *quasi*-solid-state ZIBs consisting of metallic zinc foil as anode and PVDF-$Zn(ClO_4)_2$-based polymer membrane as a *quasi*-solid electrolyte at a voltage window of 0.4–1.4 V *vs.* Zn^{2+}/Zn. The electrochemical behavior of the KHVO electrode is firstly evaluated by the cyclic voltammetry (CV) technique, as shown in Fig. 3a. One distinct pair of redox peaks locating at 0.9 and 1.0 V are observed in all four CV cycles, relating to the Zn^{2+} ions intercalation and extraction process, respectively. The redox peaks experience a slight shift with the CV shapes remained intact and stabilize from the 3rd cycle onwards, expressing high reversibility of the redox reactions for KHVO cathode. At a low current density of 100 mA/g the initial three galvanostatic charging-discharging cycles of KHVO cathode are displayed in Fig. 3b. It obtains a relatively high discharge capacity of 373 mAh/g and a charge capacity of 332 mAh/g in the first cycle, with a coulombic efficiency (CE) of 89%. The almost overlapping charging-discharging profiles for the 2nd and 3rd cycles display well-defined redox plateaus, suggesting the high reversibility of the redox reactions. Except for a slight decay during the initial few cycles, a stable and reversible specific capacity of around 300 mAh/g with 100% CE is achieved for KHVO in the following 100 cycles at 100 mA/g with a high capacity retention of 88% compared to the second cycle (Fig. 3c). In contrast, the HVO cathode shows a restricted zinc storage property at the same condition, only emerging a discharge capacity of 96 mAh/g after 100 cycles, resulting in a poor capacity retention of 45%. Furthermore, the KHVO cathode in liquid-state ZIBs also shows stable cycling performance (Fig. S5a in Supporting information), further implying the cycling stability of KHVO cathode.

Moreover, the rate capability of the KHVO cathode was also evaluated, as shown in Fig. 3d. At current densities of 0.1, 0.2, 0.5, 1, 2 and 5 A/g the reversible capacities of 270, 215, 166, 135, 110 and 65 mAh/g are achieved, respectively. On the contrary, the pure HVO cathode exhibits a relatively poor rate capability (*i.e.*, 250, 190, 133, 90 and 48 mAh/g at 0.1, 0.2, 0.5, 1 and 2 A/g, respectively) and capacity of the battery become almost undetectable when the current density increases to more than 2 A/g. In addition, the rate performance of the KHVO cathode in liquid-state ZIBs was also evaluated (Fig. S5b in Supporting information). It is can be seen that the KHVO cathode in *quasi*-solid-state ZIBs delivers an acceptable capacity retention, maintaining 70% capacity of liquid-state ZIBs even at a high rate of 5 A/g. The long-term cycling stability of both electrodes at a relatively high rate of 2 A/g are compared

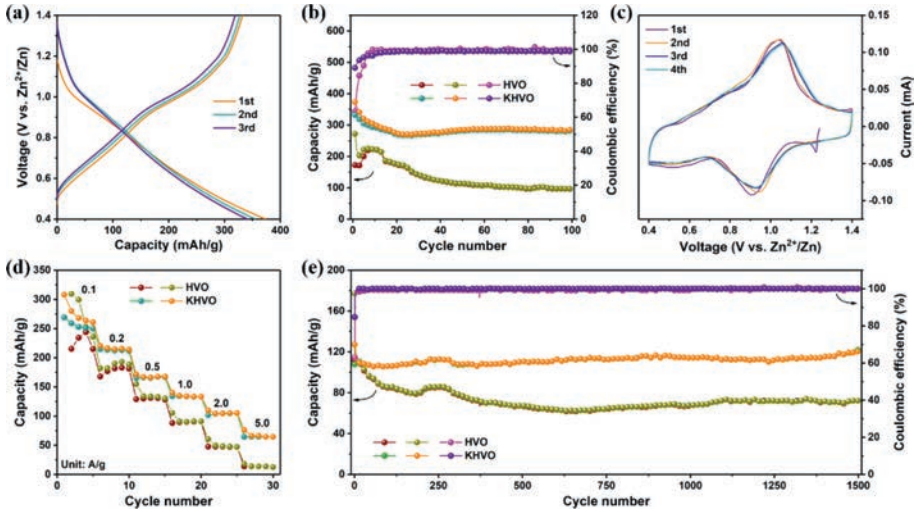

Fig. 3. (a) The initial three cycles galvanostatic charging-discharging profiles of KHVO cathode at 100 mA/g. (b) Cycling stability at 100 mA/g. (c) The first four CV curves for KHVO at 0.1 mV/s. (d) Rate property at various current densities. (e) Cycling stability at 2 A/g up to 1500 cycles.

as well. As shown in Fig. 3e, KHVO electrode exhibits almost no capacity decay throughout 1500 cycles with almost 100% CE and maintains a capacity of 120 mAh/g after 1500 cycles. The galvanostatic charging-discharging profiles of KHVO at different cycles also show almost no change (Fig. S6 in Supporting information), indicating superior reversibility and stability. While a gradual capacity decay is observed for the HVO electrode with a capacity retention of 60% after 1500 cycles at 72 mAh/g.

To find out the origin of the superior electrochemical performance of KHVO electrode comparing to HVO electrode, the apparent Zn^{2+} diffusion coefficients of both samples were calculated based on the CV technique at various scan rates (Figs. 4a and b, Fig. S7 in Supporting information). As indicated in Fig. 4a, when the scan rate increases from 0.1 mV/s to 1.0 mV/s, the position of the redox peaks for KHVO electrode shift slightly, but the overall shapes of CV curves are well maintained. As can be seen from Fig. 4b and Fig. S7b, the peak currents (i_p) are linearly related to the square root of sweeping rates ($\nu^{1/2}$), demonstrating a typical diffusion-controlled process [46,47]. After that, the diffusion coefficient of Zn^{2+} ions ($D_{Zn^{2+}}$) will be obtained by the equation as follows:

$$i_p = \left(2.69 \times 10^5\right) n^{3/2} S D_{Zn^{2+}}^{1/2} C_{Zn^{2+}} \nu^{1/2} \quad (1)$$

where n stands for the amount of charge involved in the reaction, which comes from the integral over the redox peak. S stands for the contacting area between the electrode and electrolyte. $C_{Zn^{2+}}$ stands for the Zn^{2+} concentration in the electrode material, which is determined by the ratio of Zn^{2+} involved in the reaction to the molar volume of KHVO and HVO. The main oxidation peaks marked at Fig. 4a and Fig. S7a were chosen as a representative to explore the $D_{Zn^{2+}}$. From the linear relationship between i_p and $\nu^{1/2}$ for KHVO cathode ($i_p = 0.00113\nu^{1/2} - 1.41231 \times 10^{-4}$, as shown in Fig. 4b) and HVO cathode ($i_p = 0.00581\nu^{1/2} + 4.31421 \times 10^{-5}$, as shown in Fig. S7b), $D_{Zn^{2+}}$ is calculated to be 2.27×10^{-12} cm^2/s and 1.14×10^{-13} cm^2/s for KHVO and HVO electrodes, respectively.

The galvanostatic intermittent titration technique (GITT) was also conducted, as shown in Fig. 4c and Fig. S8a (Supporting information). Based on the following equation [48–50]:

$$D_{Zn^{2+}} = \frac{4}{\pi\tau}\left(\frac{m_B V_M}{M_B S}\right)^2 \left(\frac{\Delta E_s}{\Delta E_\tau}\right)^2 \quad (2)$$

where m_B, V_M, M_B, S, τ, ΔE_s and ΔE_τ stand for the mass of electrode material, molar volume, molecular weight, geometric area of electrode, the duration of the current pulse, change of *quasi*-equilibrium potential and the change of battery voltage, respectively. The apparent Zn^{2+} ions diffusion coefficient under different charge/discharge depth are calculated to be $\sim 10^{-10}$–10^{-12} cm^2/s for KHVO cathode (Fig. 4d) and $\sim 10^{-12}$–10^{-14} cm^2/s for HVO cathode (Fig. S8b in Supporting information), respectively, which are well consistent with the above $D_{Zn^{2+}}$ determined by CV technique and further indicates the fast Zn^{2+} ions diffusion coefficient in KHVO. Besides, according to the electrochemical impedance spectroscopy analysis (Fig. S9 in Supporting information), the charge-transfer resistance of the KHVO (213 Ω) is much lower than that of HVO (572 Ω). Hence, it is believed that pre-potassiated modification contributes to the fast electrochemical kinetics of the KHVO [51–53].

Additionally, to verify the Zn^{2+} ions storage mechanism in the KHVO electrode, *ex-situ* XRD characterization at various charging-

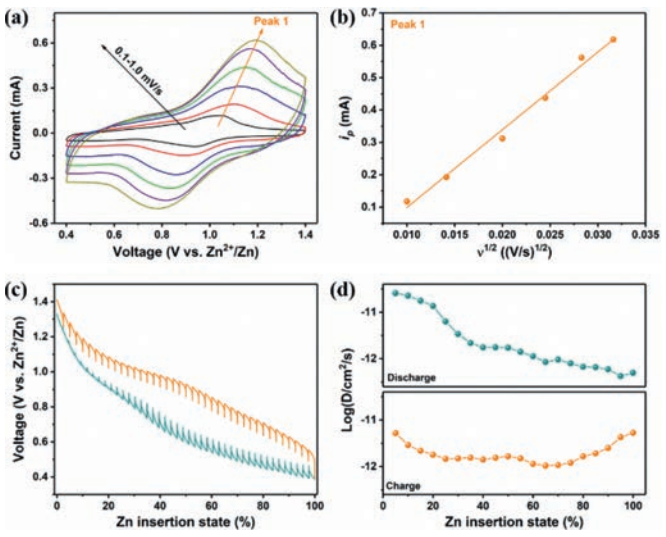

Fig. 4. (a) CV curves of KHVO cathode at various scanning rates. (b) The linear fitting of the peak current (i_p) as the *y*-axis and the square root of scanning rate ($\nu^{1/2}$) as the *x*-axis. (c) GITT profiles of KHVO cathode. (d) The calculated diffusion coefficient of Zn^{2+} in KHVO cathode.

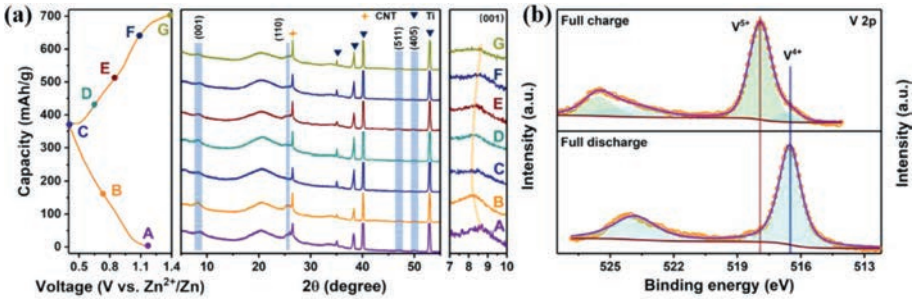

Fig. 5. (a) *Ex situ* XRD patterns of the KHVO cathode during the first cycle. (b) *Ex situ* XPS spectrum of V 2p region at the full discharge/charge states.

discharging states was carried out to explore the evolution of its crystal structure (Fig. 5a). The pristine KHVO electrode shows similar diffraction peaks of (001), (300), (511) and (405) planes to those of the KHVO powder, except for the peaks from carbon nanotubes (CNTs) (conducting material) and Ti foil (current collector). During the process of Zn^{2+} ions insertion/extraction, the same diffraction peaks as the pristine KHVO electrode are detected without generation of new diffraction peaks, evidencing the well-maintained layered KHVO crystal structure. Furthermore, a highly reversible variation of the (001) peak is evidenced, which is plotted in the enlarged (001) peak region. Upon the Zn^{2+} ions insertion, (001) peak shifts to the lower angles with an increase of the interlayer spacing. In the following Zn^{2+} ions extraction process, (001) peak gradually restores to its original position as well as the relaxation of the interlayer distance. This transition demonstrates a (de)intercalation reaction mechanism of the Zn^{2+} ion in KHVO material with superior reversibility, which can be expressed as follows: $K_{0.52}V_2O_5{\cdot}nH_2O + xZn^{2+} + xe^- \leftrightarrow Zn_xK_{0.52}V_2O_5{\cdot}nH_2O$. In addition, the XRD pattern of KHVO cathode after long cycling (Fig. S10 in Supporting information) shows no obvious change compared with original condition, indicating the superior cycling stability of KHVO electrode. To examine the vanadium chemical states at different electrochemical states the *ex-situ* XPS was also conducted (Fig. 5b). After fully discharge, only one set of characteristic peaks at 516.5 and 523.9 eV can be fitted, which belongs to the V $2p_{3/2}$ and V $2p_{1/2}$ of the V^{4+}, respectively. And when the charging is completed, the vanadium returns to its pristine V^{5+} state with V $2p_{3/2}$ and V $2p_{1/2}$ at 517.6 and 516.4 eV, respectively. Thus, based on these *ex-situ* analyses, we believe that the high stability and reversibility of KHVO electrode during the electrochemical reaction process provide a solid foundation for superior Zn storage property.

In summary, K^+ intercalation modified hydrated vanadium pentoxide ($K_{0.52}V_2O_5{\cdot}0.29H_2O$, KHVO) sample with a wrinkled 3D structure assembled by nanobelts was constructed *via* a microwave-assisted hydrothermal route. When used as cathode for *quasi*-solid-state ZIBs, the KHVO achieves an enhanced electrochemical performance of high capacity (~300 mAh/g and 88% capacity retention at 100 mA/g after 100 cycles), acceptable rate capability (110 and 65 mAh/g at 2 and 5 A/g, respectively) and ultrastable cycling performance (at 2 A/g for more than 1500 cycles). Such superior performance mainly comes from the modification of intercalated K^+, which stabilizes the lamellar structure as "pillars" and improves the Zn^{2+} ion diffusion kinetics of the electrode material.

Declaration of competing interest

The authors declare that they have no known competing financial interests or personal relationships that could have appeared to influence the work reported in this paper.

Acknowledgments

The authors gratefully acknowledge the National Natural Science Foundation of China (Nos. 51972067, 51802265, 51802044, 51902062 and 51802043), and the Guangdong Natural Science Funds for Distinguished Young Scholar (No. 2019B151502039).

Supplementary materials

Supplementary material associated with this article can be found, in the online version, at doi:10.1016/j.cclet.2021.09.091.

References

[1] Q.F. Li, X.H. Rui, D. Chen, et al., Nano-Micro Lett. 12 (2020) 1267.
[2] F. Wang, O. Borodin, T. Gao, et al., Nat. Mater. 17 (2018) 543–549.
[3] Y. Bai, H. Zhang, B. Xiang, et al., J. Colloid Interface Sci. 597 (2021) 422–428.
[4] M. Song, H. Tan, D. Chao, H.J. Fan, Adv. Funct. Mater. 28 (2018) 1802564.
[5] D. Xie, F. Hu, X. Yu, et al., Chin. Chem. Lett. 31 (2020) 2268–2274.
[6] L. Su, L. Liu, Y. Wang, et al., Chin. Chem. Lett. 31 (2020) 2358–2364.
[7] Y. Zeng, X. Zhang, Y. Meng, et al., Adv. Mater. 29 (2017) 1700274.
[8] D. Chao, C. Zhu, M. Song, et al., Adv. Mater. 30 (2018) 1803181.
[9] S. Huang, F. Wan, S. Bi, et al., Angew. Chem. Int. Ed. 58 (2019) 4313–4317.
[10] K. Leng, G. Li, J. Guo, et al., Adv. Funct. Mater. 30 (2020) 2001317.
[11] B. Tang, L. Shan, S. Liang, J. Zhou, Energy Environ. Sci. 12 (2019) 3288–3304.
[12] B. Yang, X. Cao, S. Wang, et al., Electrochim. Acta 385 (2021) 138447.
[13] W. Fan, F. Liu, Y. Liu, et al., Chem. Commun. 56 (2020) 2039–2042.
[14] L. Wang, Z. Cao, P. Zhuang, et al., ACS Appl. Mater. Interfaces 13 (2021) 13338–13346.
[15] K. Zhang, D. Kim, Z. Hu, et al., Nat. Commun. 10 (2019) 5203.
[16] Z. Li, T. Liu, R. Meng, et al., Energy Environ. Mater. 4 (2021) 111–116.
[17] Z. Liu, G. Pulletikurthi, F. Endres, ACS Appl. Mater. Interfaces 8 (2016) 12158–12164.
[18] H. Yi, R. Qin, S. Ding, et al., Adv. Funct. Mater. 31 (2021) 2006970.
[19] M. Zhang, R. Liang, T. Or, et al., Small Struct. 2 (2021) 2000064.
[20] X. Zhang, H. Chen, W. Liu, et al., Chem. Asian J. 15 (2020) 1430–1435.
[21] D. Chen, X. Rui, Q. Zhang, et al., Nano Energy 60 (2019) 171–178.
[22] C. Xia, J. Guo, Y. Lei, et al., Adv. Mater. 30 (2018) 1705580.
[23] S. Chen, K. Li, K.S. Hui, J. Zhang, Adv. Funct. Mater. 30 (2020) 2003890.
[24] W. Liu, L. Dong, B. Jiang, et al., Electrochim. Acta 320 (2019) 134565.
[25] A. Konarov, N. Voronina, J.H. Jo, et al., ACS Energy Lett. 3 (2018) 2620–2640.
[26] S. Zhao, B. Han, D. Zhang, et al., J. Mater. Chem. A 6 (2018) 5733–5739.
[27] G. Fang, C. Zhu, M. Chen, et al., Adv. Funct. Mater. 29 (2019) 1808375.
[28] A. Moretti, S. Jeong, S. Passerini, ChemElectroChem 3 (2016) 1048–1053.
[29] F. Ming, H. Liang, Y. Lei, et al., ACS Energy Lett. 3 (2018) 2602–2609.
[30] C. Liu, Z. Neale, J. Zheng, et al., Energy Environ. Sci. 12 (2019) 2273–2285.
[31] Y.J. Zhang, X.Y. Yuan, T. Lu, et al., J. Colloid Interface Sci. 585 (2021) 347–354.
[32] S. Natarajan, S.-J. Kim, V. Aravindan, J. Mater. Chem. A 8 (2020) 9483–9495.
[33] J. Sun, Y. Zhang, Y. Liu, et al., J. Colloid Interface Sci. 587 (2021) 845–854.
[34] G.S. Xu, Y.J. Zhang, Z.W. Gong, et al., J. Colloid Interface Sci. 593 (2021) 417–423.
[35] C.-Y. Lee, A.C. Marschilok, A. Subramanian, et al., Phys. Chem. Chem. Phys. 13 (2011) 18047–18054.
[36] C. Xia, J. Guo, P. Li, et al., Angew. Chem. Int. Ed. 57 (2018) 3943–3948.
[37] D. Kundu, B.D. Adams, V. Duffort, et al., Nat. Energy 1 (2016) 16119.
[38] J. Feng, Y. Wang, S. Liu, et al., ACS Appl. Mater. Interfaces 12 (2020) 24726–24736.
[39] L. Xu, Y. Zhang, J. Zheng, et al., Mater. Today Energy 18 (2020) 100509.
[40] J. He, X. Liu, H. Zhang, et al., ChemSusChem 13 (2020) 1568–1574.
[41] M. Tian, C. Liu, J. Zheng, et al., Energy Storage Mater. 29 (2020) 9–16.
[42] M. Ghosh, S. Dilwale, V. Vijayakumar, S. Kurungot, ACS Appl. Mater. Interfaces 12 (2020) 48542–48552.
[43] S. Mickevicius, V. Bondarenka, S. Grebinskij, et al., Micron 40 (2009) 126–129.

[44] S. Li, M. Chen, G. Fang, et al., J. Alloy. Compd. 801 (2019) 82–89.
[45] Y. Liu, Y. Qiao, W. Zhang, et al., Nano Energy 5 (2014) 97–104.
[46] Q. Li, D. Chen, H. Tan, et al., J. Energy Chem. 40 (2020) 15–21.
[47] X.H. Rui, D.H. Sim, C. Xu, et al., RSC Adv. 2 (2012) 1174–1180.
[48] B. Tang, G. Fang, J. Zhou, et al., Nano Energy 51 (2018) 579–587.
[49] L. Deng, X. Niu, G. Ma, et al., Adv. Funct. Mater. 28 (2018) 1800670.
[50] X. Guo, G. Fang, W. Zhang, et al., Adv. Energy Mater. 8 (2018) 1801819.
[51] Q. Li, H. Zhu, Y. Tang, et al., Chem. Commun. 55 (2019) 12108–12111.
[52] J. Liu, Y. Cao, J. Zhou, et al., ACS Appl. Mater. Interfaces 12 (2020) 54537–54544.
[53] Z. Yan, H.Y. Pan, J.Y. Wang, et al., Rare Metals 40 (2021) 1357–1365.